Electronic Supplementary Material (ESI) for Dalton Transactions.

Supplementary Information

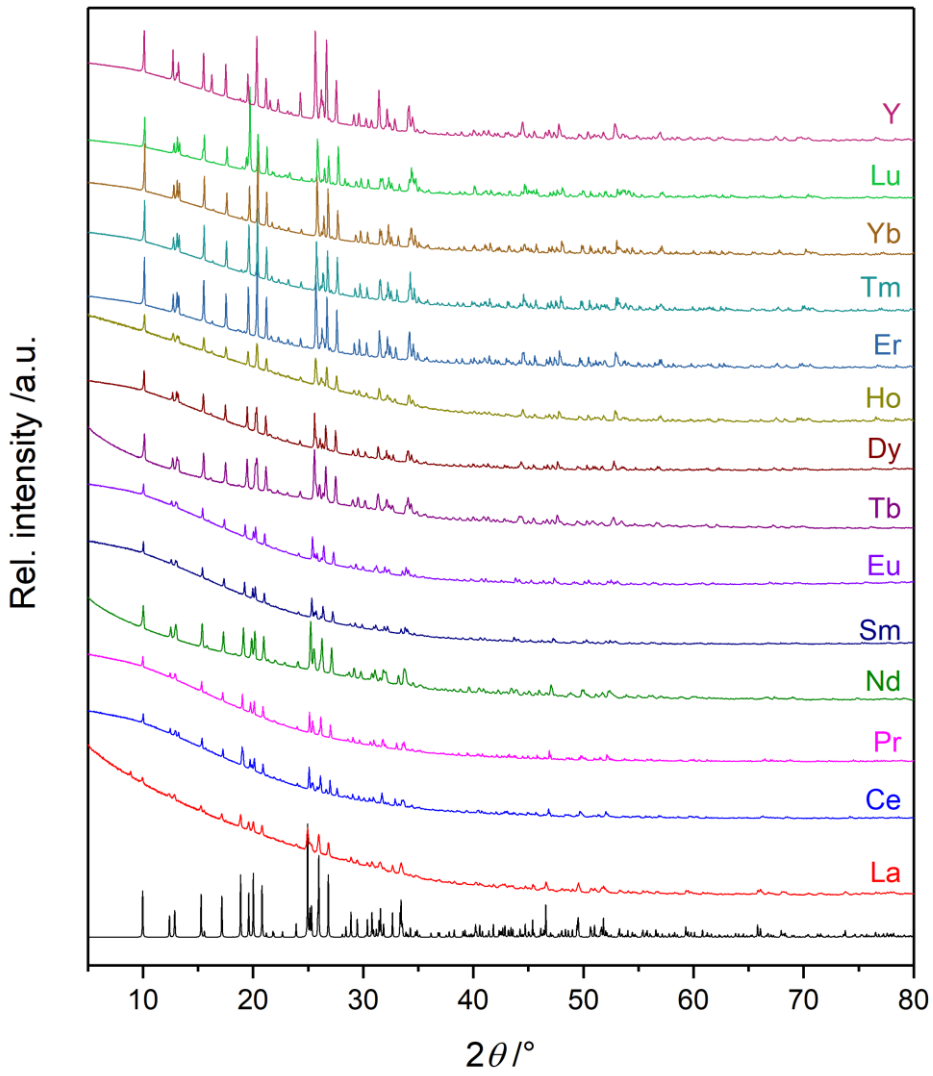

Figure S 1: PXRD pattern of $RE_2[B_2(SO_4)_6]$ (*RE* = Y, La-Nd, Sm, Eu, Tb-Lu) in comparison to the calculated pattern of $La_2[B_2(SO_4)_6]$.

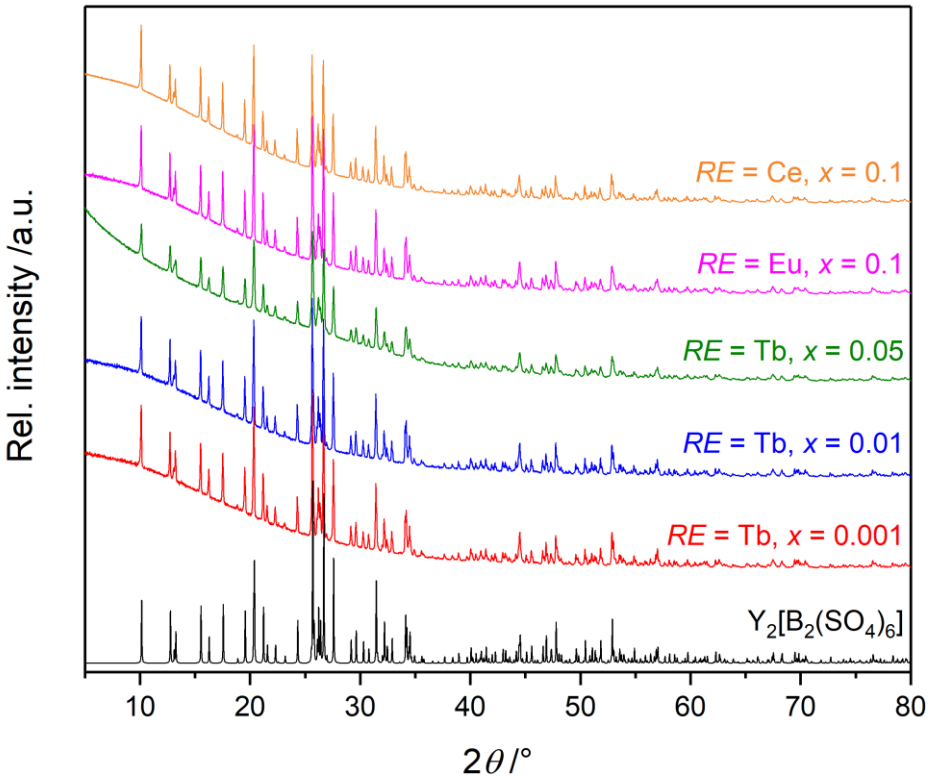

Figure S 2: PXRD pattern of doped $Y_{2-2x}RE_{2x}[B_2(SO_4)_6]$ with *RE* = Ce, Eu and Tb and *x* = 0.001-0.1 in comparison to the calculated pattern of $Y_2[B_2(SO_4)_6]$

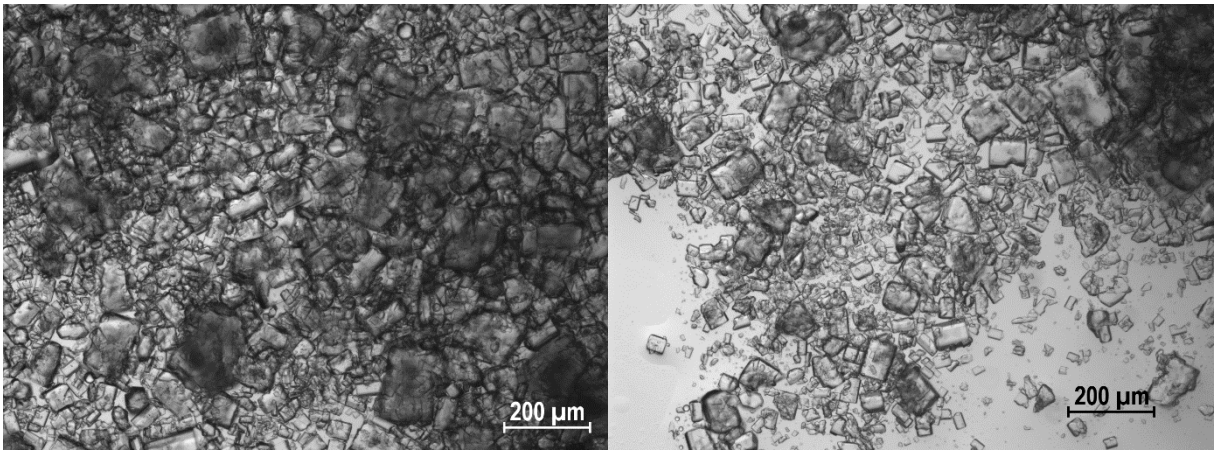

Figure S 2: Microscope images of $Ce_2[B_2(SO_4)_6]$.

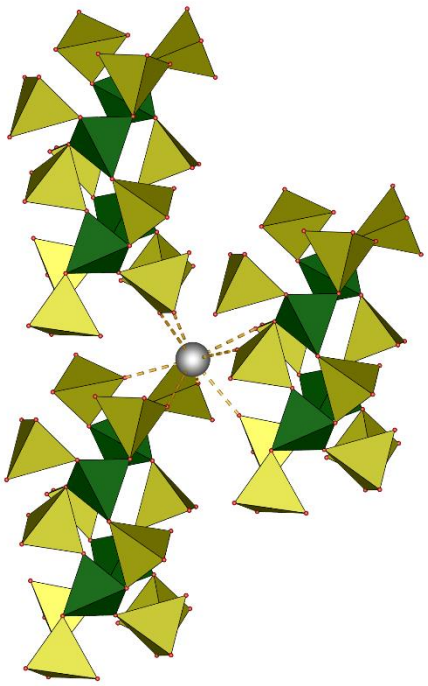

Figure S 3: Enlarged coordination environment of Eu^{3+} with complete anions.

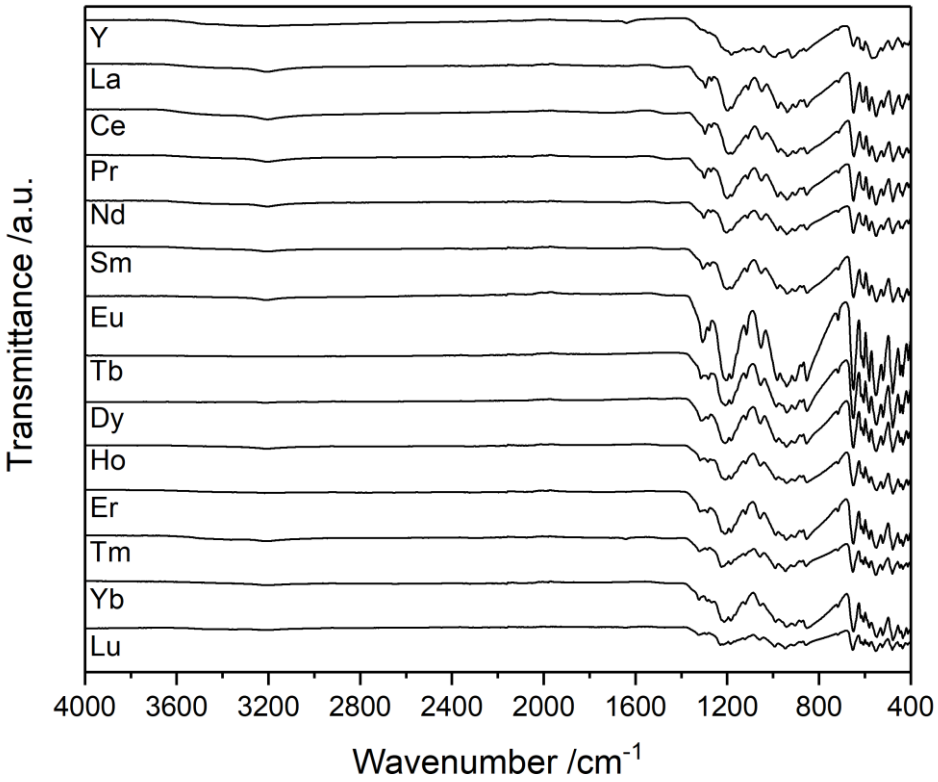

Figure S 4: Infrared spectra of $RE_2[B_2(SO_4)_6]$ (*RE* = Y, La-Nd, Sm, Eu, Tb-Lu).

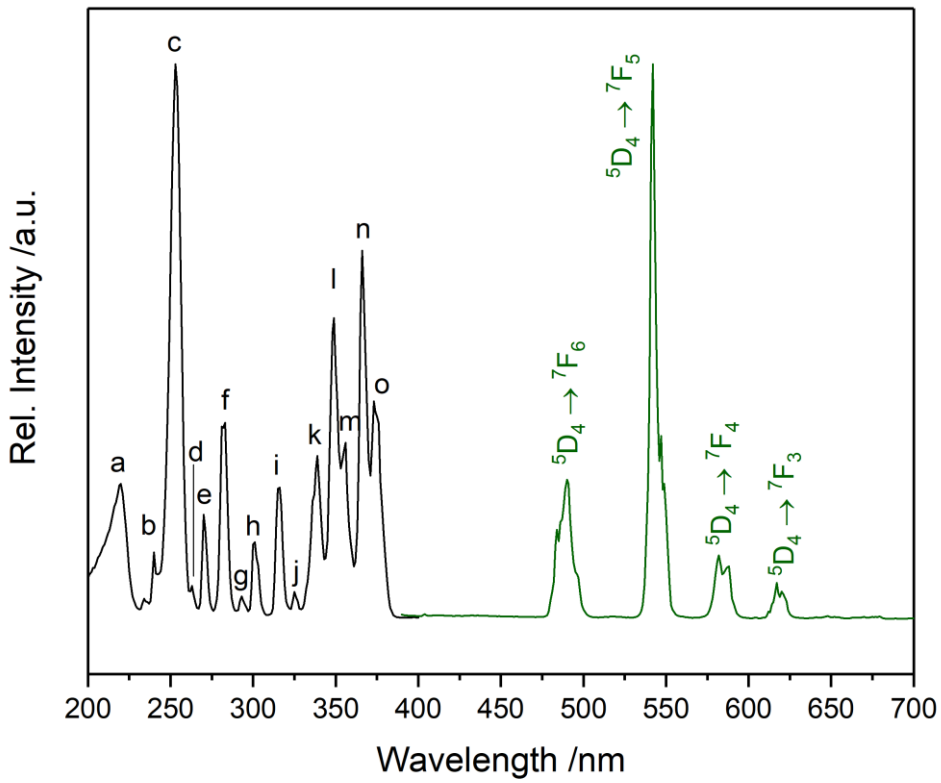

Figure S 5: Excitation ($\lambda_{em.}$ = 542 nm) and emission ($\lambda_{ex.}$ = 365 nm) spectra of $Tb_2[B_2(SO_4)_6]$. The assignment of the excitation spectra is listed in Table S1.

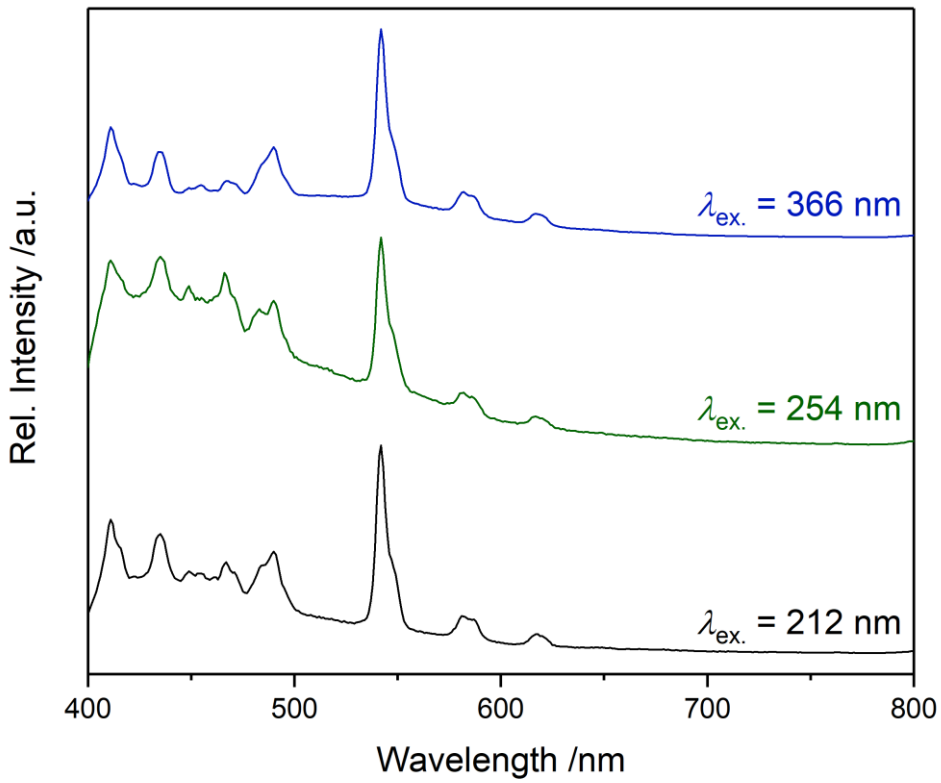

Figure S 6: Emission spectra of $Y_2[B_2(SO_4)_6]:Tb^{3+}$ (0.1 % doped) at different excitation wavelengths based on the strongest excitation bands at 212 nm (4f → 5d), 254 nm ($^7F_6 \rightarrow {}^5K_9$), and 366 nm ($^7F_6 \rightarrow {}^5L_{10}$).

Table S 1: Assignment of the excitation bands in $Tb_2[B_2(SO_4)_6]$ according to Carnall[1]

Band	Transition $^7F_6 \rightarrow$	Wavelength /nm
a	5*d*	212
b	$^5K_7$	240
c	5*d*	253
d	$^5I_6$	263
e	$^5I_7$	270
f	$^5I_8$	283
g	$^5H_5$	293
h	$^5H_6$	301
i	$^5H_7$	316
j	$^5D_1$	325
k	$^5L_7 + {}^5L_8$	339
l	$^5L_9$	349
m	$^5G_5$	356
n	$^5L_{10}$	366
o	$^5G_6$	373

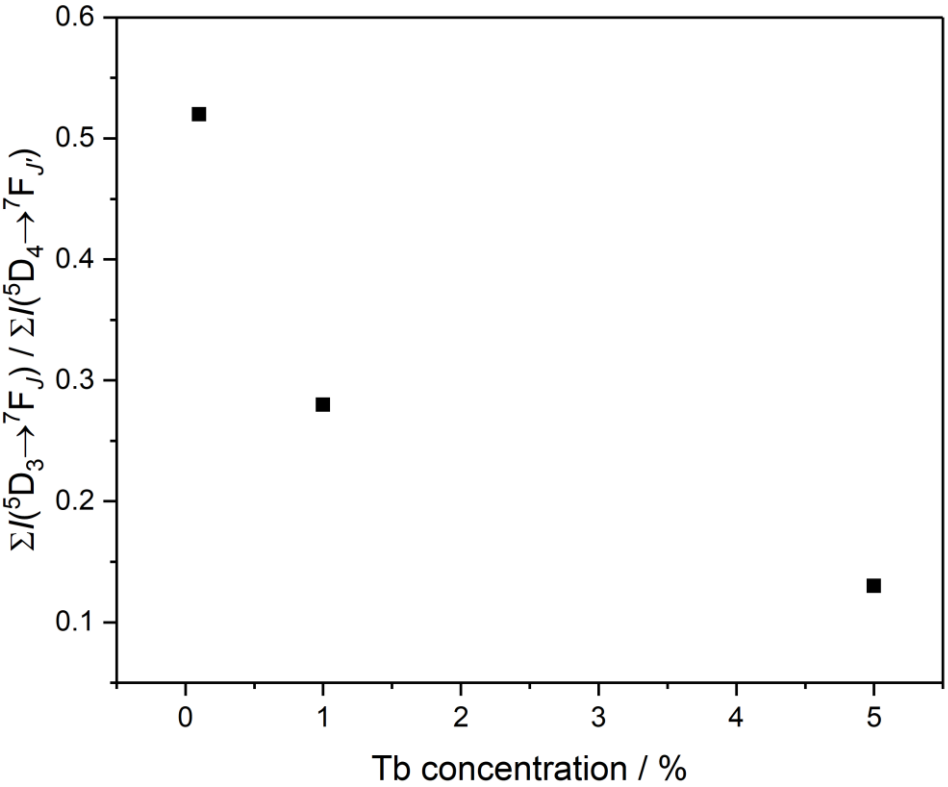

Figure S 7: Ratio of the integrated intensities $^5D_3 \rightarrow {}^7F_J$ to $^5D_3 \rightarrow {}^7F_J$ in dependence of the Tb^{3+} concentration in $Y_{2-2x}Tb_{2x}[B_2(SO_4)_6]$ with x = 0.001, 0.01 and 0.05.

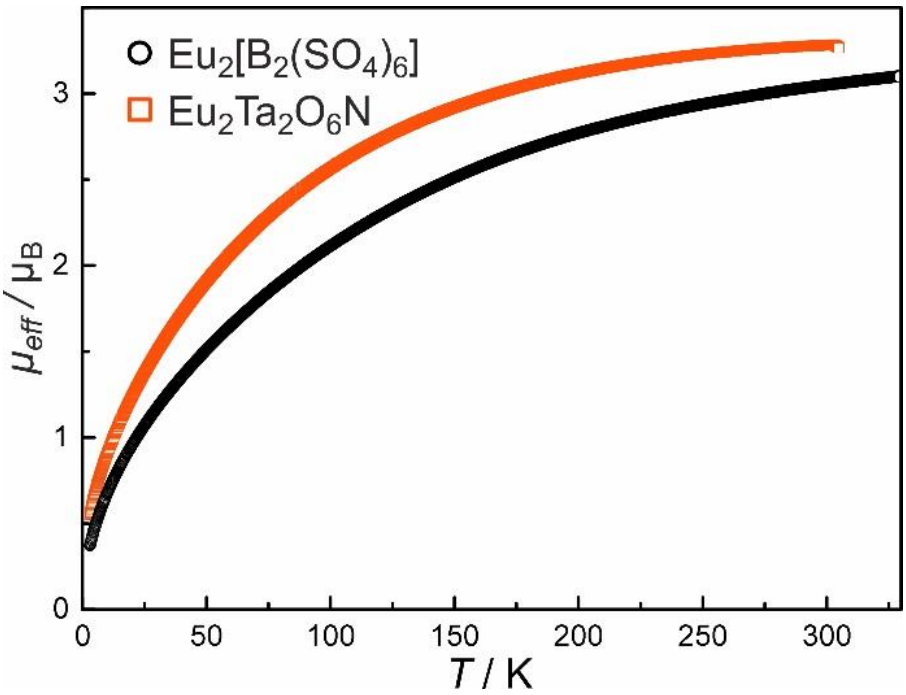

Figure S 8: Temperature dependence of the effective magnetic moment of $Eu_2[B_2(SO_4)_6]$ and $Eu_2Ta_2O_6N$[2] determined from ZFC measurements.

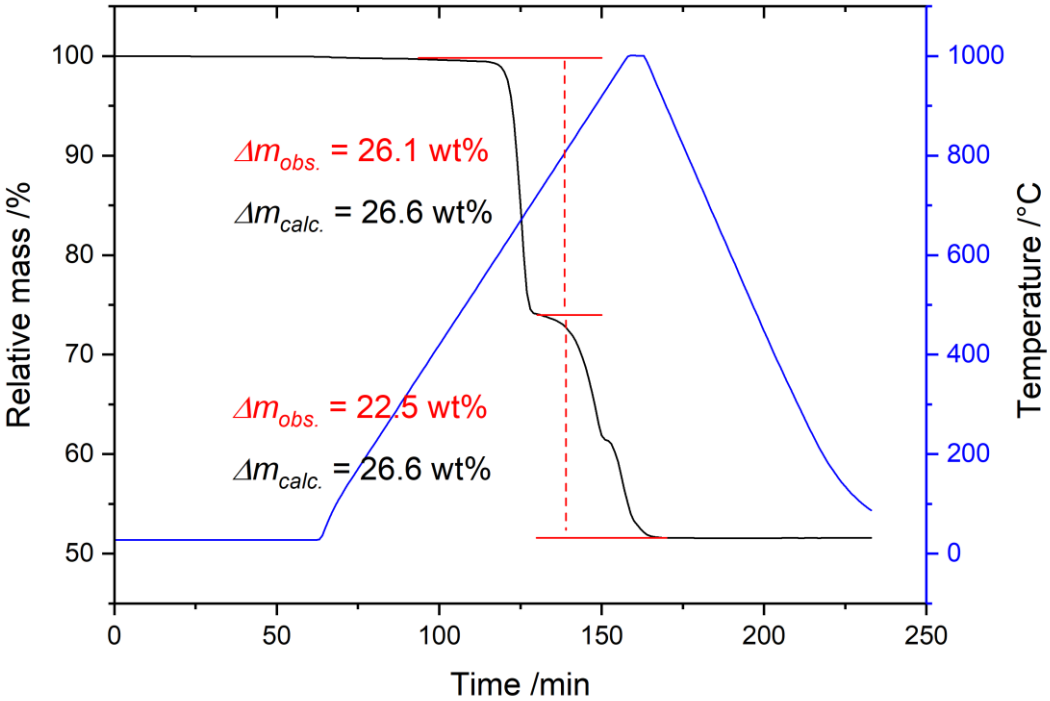

Figure S 9: Thermogram of $Eu_2[B_2(SO_4)_6]$ in dependence of the time. The second decomposition step from the sulfate to the oxide is not fully completed at 1000 °C, resulting in a slightly too low observed mass loss.

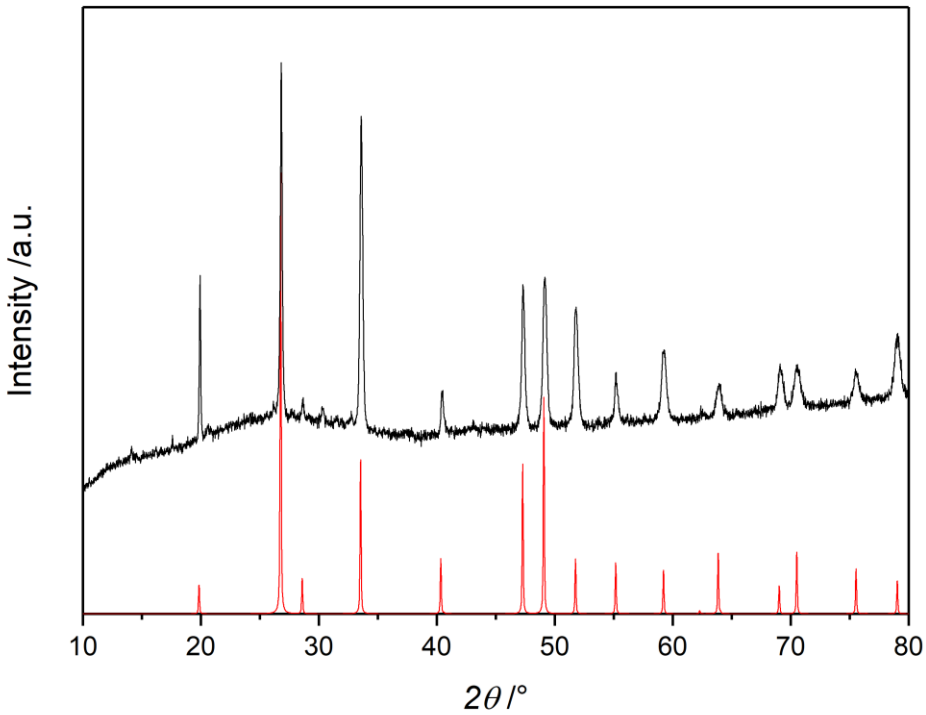

Figure S 10: PXRD of the decomposed $Eu_2[B_2(SO_4)_6]$ after 1000 °C compound in comparison to a calculated pattern of $EuBO_3$.[3]

Table S 2: Wyckoff symbol, atomic coordinates x; y; z and equivalent isotropic displacement parameters U_{eq} for $Eu_2[B_2(SO_4)_6]$ (corresponding standard deviations given in parentheses)

Atom	Wyckoff symbol	*x*	*y*	*z*	U_{eq}
Eu1	8*f*	0.18779(3)	0.95165(3)	0.15554(3)	0.00581(11)
S1	8*f*	0.13794(14)	1.20181(16)	0.36121(16)	0.0063(4)
S2	8*f*	0.12790(14)	0.51284(16)	0.07698(16)	0.0065(4)
S3	8*f*	-0.07760(14)	0.85044(16)	0.08057(16)	0.0071(4)
O11	8*f*	0.1798(4)	1.1576(4)	0.4756(4)	0.0111(8)
O12	8*f*	0.1211(4)	1.1105(4)	0.2720(5)	0.0111(8)
O13	8*f*	0.1959(4)	1.2983(5)	0.3169(5)	0.0124(12)
O14	8*f*	0.0339(4)	1.2495(5)	0.3825(4)	0.0085(11)
O21	8*f*	0.1765(4)	0.4812(4)	-0.0292(5)	0.0125(12)
O22	8*f*	0.1865(4)	0.5179(4)	0.1887(5)	0.0109(12)
O23	8*f*	0.0813(4)	0.6321(4)	0.0607(5)	0.0125(12)
O24	8*f*	0.0419(4)	0.4311(4)	0.0961(5)	0.0094(12)
O31	8*f*	0.0202(4)	0.8850(5)	0.1210(5)	0.0182(13)
O32	8*f*	0.1154(5)	1.0840(5)	0.0233(5)	0.0212(14)
O33	8*f*	-0.1471(4)	0.8491(5)	0.1743(5)	0.0132(12)
O34	8*f*	-0.0748(4)	0.7228(4)	0.0404(5)	0.0120(12)
B1	8*f*	0.0006(7)	0.6700(7)	-0.0271(7)	0.0081(18)

Table S 3: Anisotropic displacement parameters U_{ij} in $Å^2$ for $Eu_2[B_2(SO_4)_6]$ (corresponding standard deviations given in parentheses)

Atom	U_{11}	U_{22}	U_{33}	U_{23}	U_{13}	U_{12}
Eu1	0.0045(2)	0.00707(18)	0.00596(17)	-0.00037(17)	0.00133(12)	0.00053(18)
S1	0.0050(10)	0.0059(9)	0.0082(9)	0.0000(7)	0.0020(7)	-0.0007(7)
S2	0.0058(10)	0.0060(9)	0.0077(9)	0.0014(7)	0.0005(7)	-0.0015(7)
S3	0.0063(10)	0.0086(9)	0.0067(9)	-0.0008(7)	0.0020(7)	0.0003(7)
O11	0.011(2)	0.0110(19)	0.0112(19)	-0.0047(15)	-0.0005(15)	0.0061(17)
O12	0.011(2)	0.0110(19)	0.0112(19)	-0.0047(15)	-0.0005(15)	0.0061(17)
O13	0.009(3)	0.014(3)	0.015(3)	0.002(2)	0.004(2)	-0.003(2)
O14	0.006(3)	0.013(3)	0.006(3)	-0.002(2)	-0.003(2)	0.001(2)
O21	0.009(3)	0.010(3)	0.020(3)	-0.003(2)	0.008(2)	-0.005(2)
O22	0.011(3)	0.010(3)	0.011(3)	0.001(2)	-0.003(2)	-0.004(2)
O23	0.012(3)	0.007(3)	0.018(3)	0.002(2)	0.001(2)	-0.001(2)
O24	0.011(3)	0.005(3)	0.014(3)	-0.002(2)	0.006(2)	-0.002(2)
O31	0.016(4)	0.025(3)	0.014(3)	-0.011(3)	0.004(2)	-0.009(3)
O32	0.026(4)	0.022(3)	0.016(3)	0.012(2)	0.004(3)	0.012(3)
O33	0.007(3)	0.022(3)	0.012(3)	-0.004(2)	0.007(2)	-0.004(2)
O34	0.009(3)	0.009(3)	0.019(3)	-0.002(2)	0.008(2)	-0.002(2)
B1	0.010(5)	0.005(4)	0.009(4)	-0.003(3)	0.004(3)	0.000(3)

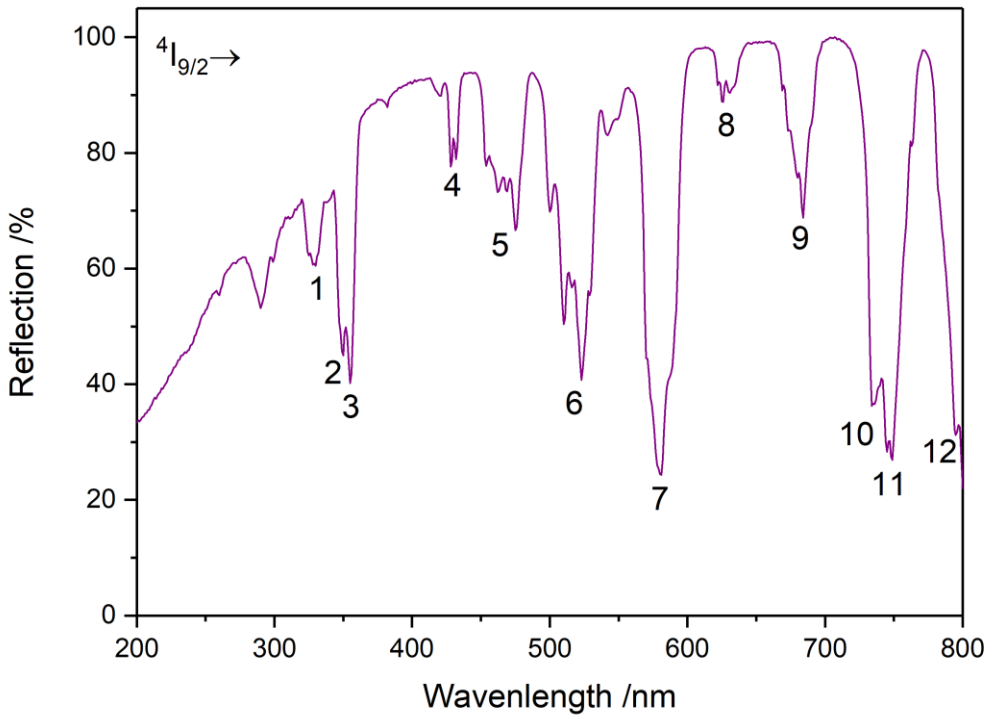

Figure S 11: Reflection spectrum of $Nd_2[B_2(SO_4)_6]$.The transitions originating from the ground state $^4I_{9/2}$ are assigned in table S 4.

Table S 4: Assignment of the transitions in Fig. S11 according to Carnall[4]

Band	Transition $^4I_{9/2} \longrightarrow$	Wavelength /nm
1	$^2I_{13/2} + {}^4D_{7/2} + {}^2L_{17/2}$	330
2	$^4D_{5/2} + {}^4D_{3/2}$	350
3	$^4D_{1/2} + {}^2I_{11/2} + {}^2I_{15/2}$	355
4	$^2P_{1/2} + {}^2D_{5/2}$	430
5	$^2K_{15/2} + {}^2G_{9/2} + {}^2D_{3/2} + {}^4G_{11/2}$	450-480
6	$^2K_{13/2} + {}^4G_{7/2} + {}^4G_{9/2}$	500-530
7	$^5G_{5/2} + {}^2G_{7/2}$	581
8	$^2H_{11/2}$	626
9	$^4F_{9/2}$	684
10	$^4S_{3/2}$	734
11	$^4F_{7/2}$	749
12	$^2H_{9/2}$	795

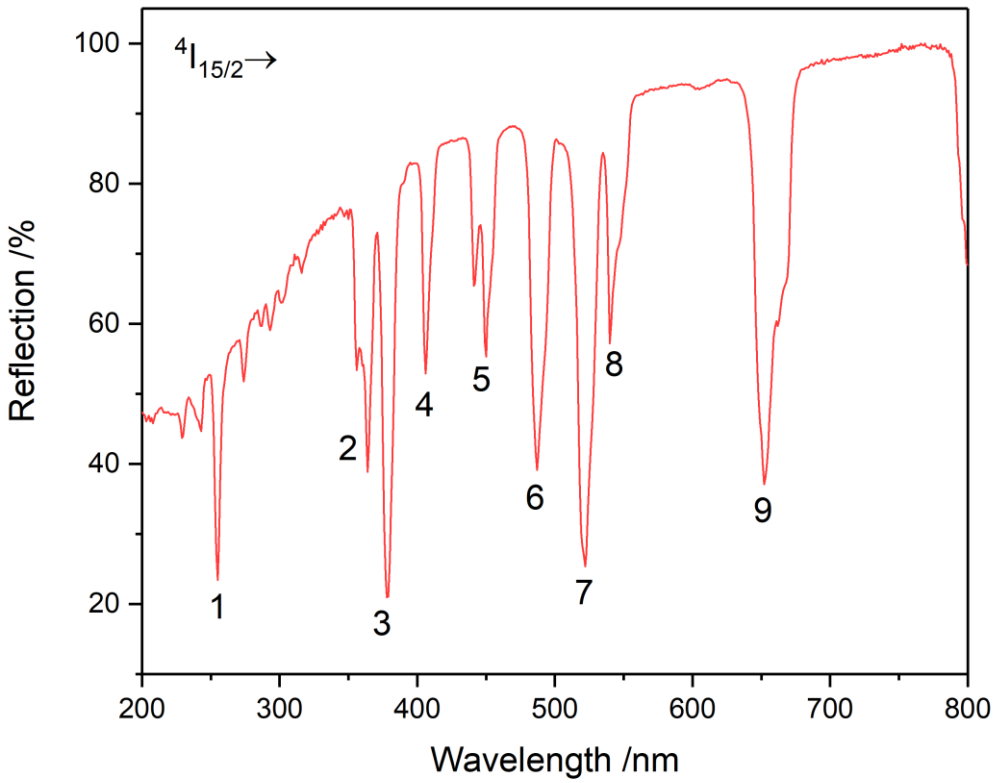

Figure S 12: Reflection spectrum of $Er_2[B_2(SO_4)_6]$.The transitions originating from the ground state $^4I_{15/2}$ are assigned in table S 4.

Table S 5: Assignment of the transitions in Fig. S11 according to Carnall[4]

Band	Transition $^4I_{15/2} \longrightarrow$	Wavelength /nm
1	$^4D_{7/2}$	255
2	$^4G_{9/2}$	364
3	$^4G_{11/2}$	378
4	$(^2G, ^4F)_{9/2}$	406
5	$^4F_{5/2}$	450
6	$^4F_{7/2}$	487
7	$(^2H, ^4G)_{11/2}$	581
8	$^4S_{3/2}$	626
9	$^4F_{9/2}$	684

References

[1] W. T. Carnall, P. R. Fields, K. Rajnak, *J. Chem. Phys.* **1968**, *49*, 4447–4449.
[2] B. Anke, S. Hund, C. Lorent, O. Janka, T. Block, R. Pöttgen, M. Lerch, *Z. anorg. allg. Chem.* **2017**, *643*, 1824–1830.
[3] R. E. Newnham, M. J. Redman, R. P. Santoro, *J. Am. Ceram. Soc.* **1963**, *46*, 253–256.
[4] W. T. Carnall, P. R. Fields, K. Rajnak, *J. Chem. Phys.* **1968**, *49*, 4424–4442.